analytical chemistry

pubs.acs.org/ac Article

Novel Ratiometric Electrochemiluminescence Biosensor Based on BP-CdTe QDs with Dual Emission for Detecting MicroRNA-126

Jinwen Zhao, Ying He, Kejun Tan, Jun Yang, Shihong Chen,* and Ruo Yuan

Cite This: *Anal. Chem.* 2021, 93, 12400−12408 Read Online

ACCESS | Metrics & More | Article Recommendations | Supporting Information

ABSTRACT: The electrochemiluminescence (ECL) ratiometric assay is usually based on two different ECL luminophores, and the choice of two suitable luminophores and shared co-reactant makes its construction challenging. The single-emitter-based ECL ratio mode could overcome the limitation of two luminophores and simplify the construction process, so it is an ideal choice. In this work, CdTe quantum dots (CdTe QDs) were modulated using black phosphorus (BP) nanosheet to simultaneously emit the cathodic and anodic ECL signals, and H_2O_2 and tripropylamine (TPrA) served as the cathodic and anodic co-reactants, respectively. MicroRNA-126 (miRNA-126) was selected as the template target to exploit the application of BP-CdTe QDs in the single-emitter-based ECL ratio detection. Through the target recycling triggering rolling-circle amplification (RCA) reaction, a large amount of glucose oxidase (GOx)-modified single strand 1 was introduced. GOx catalyzed glucose to produce H_2O_2 in situ, which acted as a dual-role moderator to quench the anodic ECL emission with TPrA as the co-reactant while enhancing the cathodic emission, thereby realizing the ratiometric detection of miRNA-126 with a low detection limit of 29 aM (S/N = 3). The dual-ECL-emitting BP-CdTe QDs with TPrA-H_2O_2 as dual co-reactant provide a superior ECL ratio platform involving enzyme catalytic reaction, expanding the application of single-emitter-based ratio sensing in the diverse biological analysis.

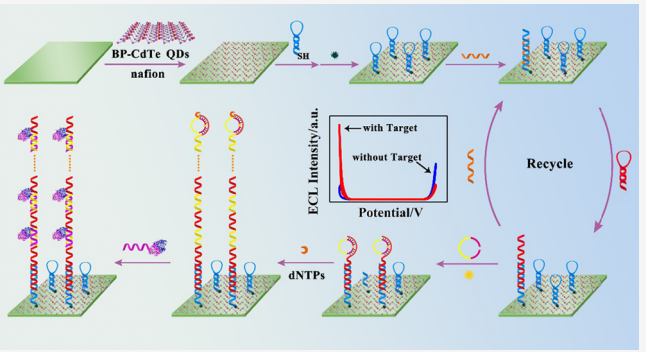

INTRODUCTION

Electrochemiluminescence (ECL) is gaining more and more applications in drug and food detection, clinical diagnosis, and environmental monitoring due to its rapid response, high sensitivity, low background signal, and wide dynamic range.[1,2] Compared to the traditional single-signal ECL measurement, the ECL ratiometric strategy has caught researchers' widespread attention as it could eliminate ambiguous inference by self-calibration of two signals under a complex biological environment.[3] The two ECL signals in ratiometric strategy may come from two different ECL luminophores or from the same luminophore. Most ECL ratiometric strategies are based on the first mode. In this case, two ECL luminophores are either encapsulated independently and introduced into the ECL system in steps,[4,5] or encapsulated as a composite and introduced into the ECL system simultaneously.[6] For example, Xu's group separately introduced Au-g-C_3N_4 and $Ru(bpy)_3^{2+}$ to construct an ECL ratio biosensor for detecting miRNA-21 through the resonance energy transfer (RET) between two luminophores.[7] In our previous work, the cathodic luminophore (RGO-CdTe quantum dots (QDs)) and anodic luminophore (PFO dots) were encapsulated as a composite to construct an enzyme-based inhibition biosensor, which achieved the ECL ratio detection of organophosphorus pesticides by consuming cathodic co-reactant-dissolved O_2 and generating anodic co-reactant H_2O_2 during the enzyme catalytic reaction.[8] In addition, CdSQDs and MOF-5 were also encapsulated as a composite for the ECL ratio detection of cTnI.[9] It is challenging to select two luminophores whose signals have different change trends for ratio detection. The single-emitter-based ECL ratio mode could avoid the tedious work of searching for two well-matched luminophores and elaborating their composite, simplify the construction process, and save experimental cost, making it an attractive choice.

Among the commonly used ECL luminophores, only a few of the luminophores could simultaneously emit the cathodic and anodic ECL signals for constructing the single-emitter-based ratio sensing. For example, Li's group developed the nitrogen-doped graphene quantum dots with dual-signal output for the ratiometric ECL detection of Co^{2+} and nicotinamide adenine dinucleotide (NADH), respectively.[10,11] Cao et al. regulated the dual emission of $Ru(bpy)_3^{2+}$ for the

Received: June 7, 2021
Accepted: August 20, 2021
Published: September 1, 2021

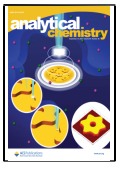

https://doi.org/10.1021/acs.analchem.1c02408
Anal. Chem. 2021, 93, 12400−12408

Scheme 1. (A) Preparation of BP-CdTe QDs. (B) Conjugation of GOx to S1. (C) Fabrication of the Biosensor for miRNA-126 Detection

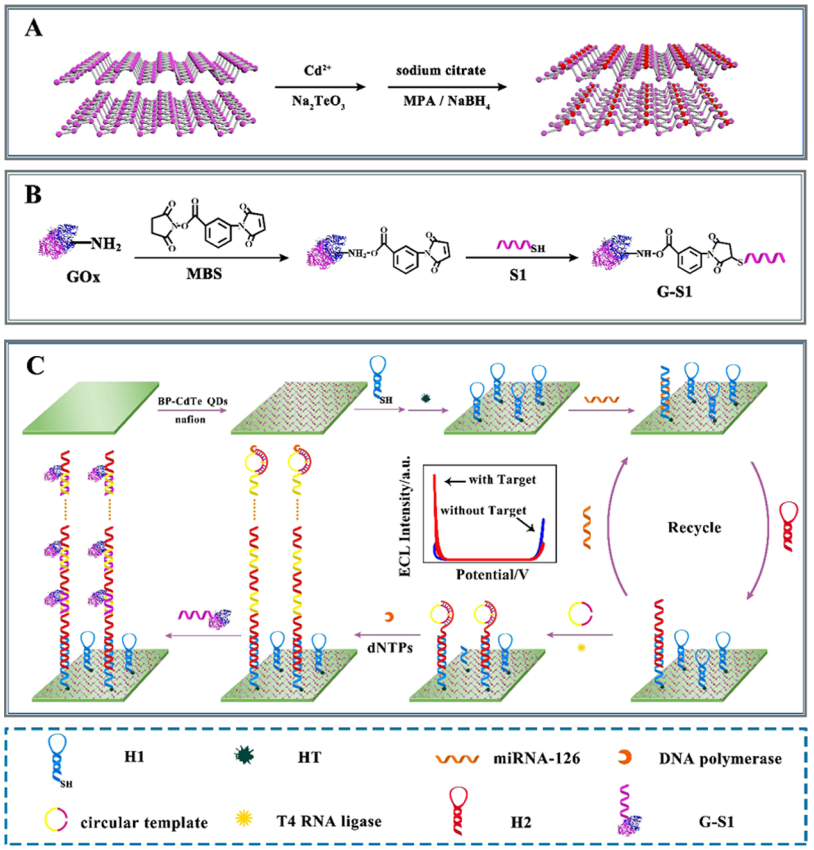

ratiometric detection of Hg^{2+}.[12] Additionally, graphitic carbon nitride quantum dots were exploited to emit two different ECL signals for the ratiometric detection of ascorbic acid.[13] Those reported single-emitter-based ECL ratio systems generally required specific targets such as Co^{2+}, Hg^{2+}, NADH, or ascorbic acid to change the intensity of two signals, thus greatly limiting their application. It is of great significance to develop a superior single luminophore with a dual-signal output capability to extend the application of single-emitter-based ratio sensing.

For the construction of an ECL ratiometric sensing strategy, in addition to the selection of luminophores, the selection of co-reactants is also very challenging. In the currently reported ECL ratio strategy, two luminophores usually shared the same co-reactant, and the different variations of two signals were achieved through either the competitive consumption of a shared co-reactant or the RET. The shared co-reactant was commonly limited to H_2O_2, dissolved O_2, or $S_2O_8^{2-}$.[14,15] Moreover, the accuracy problems caused by the competitive consumption of the co-reactant and the distance-dependent problem of RET limit the application of the ECL ratio mode. To overcome the limitation of the single co-reactant, dual co-reactants have been developed for ECL ratiometric detection, including $S_2O_8^{2-}$-H_2O_2, dissolved O_2-$S_2O_8^{2-}$, $S_2O_8^{2-}$-amine, dissolved O_2-amine, and dissolved O_2-H_2O_2.[8,13,15−17] Obviously, the application of $S_2O_8^{2-}$ or dissolved O_2 was usually involved in those reported dual-co-reactant systems. The uncertainty of dissolved O_2 concentration and strong oxidation of $S_2O_8^{2-}$ inevitably leads to instability or repeatability problems. Moreover, the exogenous moderator such as CyS, polyaniline, Ni^{2+}, or Cu_2O was needed to regulate the different changes in two signals. The addition of the moderator would increase the difficulty in the construction of sensing strategies and the complexity of detection systems. Since H_2O_2 could not only act as the cathodic co-reactant[18] but also quench the anodic ECL emission with tripropylamine (TPrA) as the co-reactant,[19] thus it is a superior dual-role moderator to facilitate the different variations of two signals. The combination of H_2O_2 generated in situ through enzyme-catalyzed reaction and TPrA as a dual co-reactant would facilitate the improvement of stability and repeatability, overcome the complexity caused by the introduction of exogenous moderator, thus showing a great potential application in dual-co-reactant-based ratio systems. At present, TPrA-H_2O_2 as dual co-reactant for ratiometric biosensors has not been reported yet.

CdTe QDs have been getting increasing attention in the ECL assay owing to their high quantum yield, stable light emission, and good biocompatibility.[20,21] The cathodic ECL emission of CdTe QDs has been studied extensively, either for single-signal detection or ratio detection.[8,22] Meanwhile, the anodic ECL emission of CdTe QDs has also been studied and applied for biosensing.[23,24] The cathodic and anodic emission characteristics of CdTe QDs made it potentially capable of constructing single-emitter-based ratio modes. The dual emission of CdTe QDs during continuous signal scanning has not been reported yet. The reason might be as follows. On the one hand, it is difficult to find well-matched double co-reactant for improving the ECL emissions from the cathode and anode, respectively. On the other hand, even if two powerful ECL emissions could be obtained, it is still difficult to

https://doi.org/10.1021/acs.analchem.1c02408
Anal. Chem. 2021, 93, 12400−12408

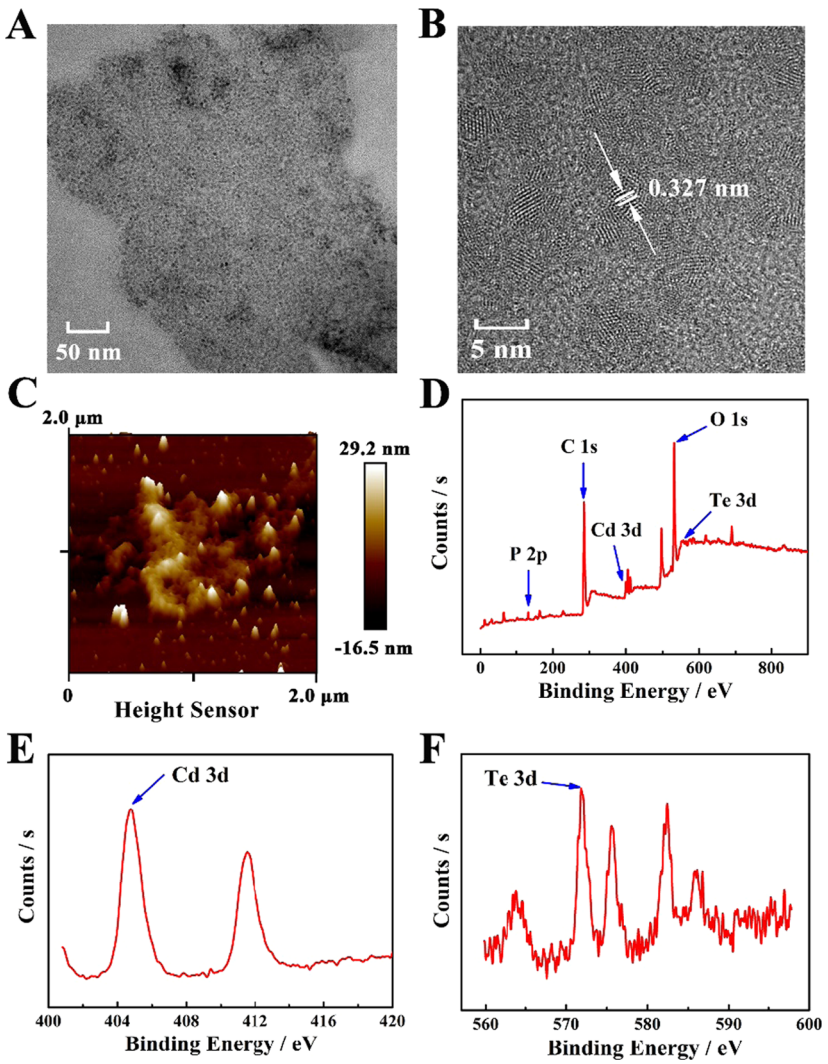

Figure 1. (A) TEM graph, (B) high-resolution TEM (HRTEM) graph, (C) AFM graph, and (D) X-ray photoelectron spectroscopy (XPS) spectra of BP-CdTe QDs. (E) Cd 3d region and (F) Te 3d region of XPS spectra.

find a dual-role moderator to achieve different changes in two emissions for the ratiometric assay.

The black phosphorus (BP) nanosheet has high carrier mobility and a large specific surface area.[25,26] It could not only achieve high loading of CdTe QDs but also increase the conductivity of the electrode interface and facilitate the electron transfer. In this work, it was innovatively developed to modulate the dual emission of CdTe QDs with TPrA-H_2O_2 as a dual co-reactant. Due to the significant role in the assessment of heart failure and maintenance of vascular integrity,[27,28] miRNA-126 was selected as the template target to exploit the application of the BP-nanosheet-equipped CdTe QDs (BP-CdTe QDs) in the single-emitter-based ECL ratio strategy. As shown in Scheme 1, BP-CdTe QDs were first prepared and used as the matrix to immobilize the SH-modified hairpin (H1) through the Cd−S covalent bond. Then, the catalytic hairpin assembly (CHA) was triggered by the target miRNA-126 to provide the binding site for the circular template of rolling-circle amplification (RCA). The RCA reaction was further activated in the presence of the polymerase, dNTPs, and circular template to produce a large number of RCA products with binding sites for glucose oxidase (GOx)-modified single strand 1 (G-S1). With the introduction of G-S1, the substrate glucose was catalyzed by GOx to generate H_2O_2, which served as a dual-role moderator to quench the anodic ECL signal with the co-reactant TPrA and enhance the cathodic signal from BP-CdTe QDs, thus realizing the ratio detection of miRNA-126. The integration of dual-ECL-emitting BP-CdTe QDs with dual co-reactant TPrA-H_2O_2 provides a preeminent single-emitter-based ECL ratiometric sensing platform for detecting diverse biomolecules.

EXPERIMENTAL SECTION

Reagents, Materials, and Apparatus. Reagents, materials, and instruments used in this work are presented in the Supporting Information. The information on the nucleic acid sequences and modifications is also illustrated in Table S1 in the Supporting Information.

Preparation of BP Nanosheet. The BP nanosheet was prepared from the bulk BP by liquid exfoliation. Briefly, 10 mg of bulk BP powder was added in 10 mL of *N*-methyl-2-pyrrolidone (NMP). After the mixture was sonicated in an ice bath for 10 h, the resultant mixture underwent natural sedimentation for 24 h to remove the nonexfoliated bulk BP. Then, the obtained supernatant was centrifuged for 10 min at

https://doi.org/10.1021/acs.analchem.1c02408
Anal. Chem. 2021, 93, 12400−12408

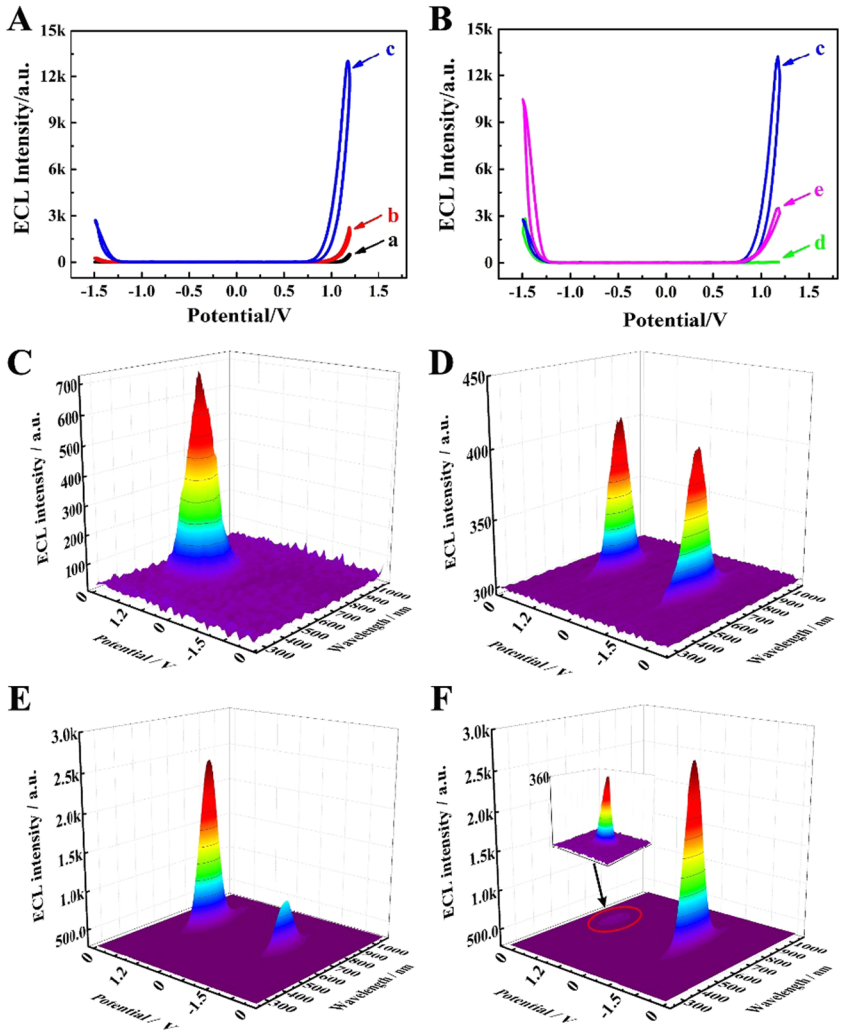

Figure 2. (A, B) ECL response of (a) BP/GCE, (b) Cd Te QDs/GCE, and (c) BP-CdTe QDs/GCE with 10 mM TPrA alone, (d) BP-CdTe QDs/GCE without TPrA and H_2O_2, and (e) BP-CdTe QDs/GCE with 10 mM TPrA and 5.0 mM H_2O_2. Three-dimensional (3D) ECL spectra of (C) BP/GCE, (D) CdTe QDs/GCE, (E) BP-CdTe QDs/GCE with 10 mM TPrA alone, and (F) BP-CdTe QDs/GCE with 10 mM TPrA and 10 mM H_2O_2 (insets: enlarged anodic 3D ECL spectra). Detection solution: 0.10 M PBS solution (pH 7.4). Scanning potential range: −1.5 to +1.2 V.

4000 rpm and the few-layer BP nanosheet dispersion was achieved by collecting the supernatant.

Preparation of BP-CdTe QDs. Scheme 1A depicts the synthesis process of BP-CdTe QDs. First, 36.89 mg of $CdCl_2 \cdot 2.5H_2O$ and 1 mL of BP nanosheet dispersion were added to 50 mL of ultrapure water. After the mixture was stirred for 1 h, Na_2TeO_3 (0.010 M, 1 mL), 3-mercaptopropionic acid (MPA) (33 μL), sodium citrate (50 mg), and $NaBH_4$ (100 mg) were added gradually into the above mixture. The resultant mixture was refluxed at 130 °C for 8 h to grow CdTe QDs on the BP nanosheet. The resultant BP-CdTe QDs were centrifuged (12 000 rpm, 5 min) and washed three times with ethanol. The collected BP-CdTe QDs were dispersed in 5.0 mL of ultrapure water and kept at 4 °C for later use.

Conjugation of GOx to S1. The conjugation of glucose oxidase (GOx) to SH-modified S1 was performed according to the method reported in the literature.[19] First, to reduce the disulfide bond of SH-modified S1, it was treated with 10 mM tris(2-carboxyethyl) phosphine (TCEP) at room temperature for 1 h. Then, 25 μL of 6.4 mM maleimidobenzoic acid *N*-hydroxy-succinimide ester (MBS) and 1 mL of 1.0 mg/L GOx were mixed and reacted at room temperature for 1 h to prepare MBS-activated GOx. Finally, the MBS-activated GOx was added to 100 μL of the as-treated S1 (20 μM). The resultant solution reacted for 1 h to prepare the conjugate of GOx and SH-modified S1 (G-S1). In such a preparation process, MBS served as the cross-linking agent and could specifically cross-link primary amines of GOx with sulfhydryl groups of SH-modified S1 to form the conjugate G-S1. Scheme 1B depicts the synthesis process and principle of G-S1.

Fabrication of the Biosensor. Scheme 1C depicts the fabrication of the biosensor. After the glassy carbon electrode (GCE) with 4.0 mm diameter was polished using alumina powder and cleaned thoroughly with ultrapure water, it was modified with 5.0 μL of Nafion (0.5%) and 10 μL of BP-CdTe QDs dispersion. Then, the BP-CdTe QDs/GCE was dried at room temperature and further incubated with 15 μL of H1 (2 μM) at 4 °C for 14 h to form the Cd−S bond between H1 and BP-CdTe QDs. After its nonspecific binding sites were blocked through incubating with HT (1.0 mM) for 1 h at 4 °C, the modified electrode was further incubated with H2 (2.0 μM, 5.0 μL) and miRNA-126 (5.0 μL) for 2 h at 37 °C to implement the target-induced CHA process, followed by incubation at 37 °C for 1 h with 15 μL of the mixture solution, which contained

https://doi.org/10.1021/acs.analchem.1c02408
Anal. Chem. 2021, 93, 12400−12408

1 × T4 DNA ligase reaction buffer, 5.0 μM circular template, and 5 U T4 DNA ligase. With the further incubation of the mixture solution containing 2.5 mM dNTPs, 1 × Phi29 DNA polymerase buffer, and 2 U Phi29 DNA polymerase on the electrode at 37 °C for 2 h, the RCA reaction was initiated. Finally, the electrode was incubated with 10 μL of G-S1 (10 μM) for 2 h at room temperature. For each modification step, the electrodes were washed with pH 7.4 phosphate-buffered saline (PBS) solution. The electrochemical impedance spectroscopy (EIS) and cyclic voltammetry (CV) were used to confirm the successful assembly of the biosensor. The corresponding figures (Figure S1) and descriptions are presented in the Supporting Information.

ECL Measurement of the Biosensor. The ECL response of the constructed ratio biosensor was detected in 2.0 mL of the PBS solution (0.10 M, pH 7.4) containing 2.0 mM glucose and 10 mM TPrA. The following test conditions were used, including the voltage of 800 V for the photomultiplier, the scanning rate of 300 mV/s, and the scanning potential range from −1.5 to +1.2 V.

RESULTS AND DISCUSSION

Characterization of BP-CdTe QDs. A transmission electron microscope (TEM) and an atomic force microscope (AFM) were used to characterize the morphology of BP-CdTe QDs. As displayed in the TEM images (Figure 1A), a large amount of evenly dispersed CdTe QDs was observed on the surfaces of the BP nanosheet. The high-resolution TEM image (Figure 1B) exhibited the crystal structure of BP-CdTe QDs with a clear lattice fringe of 0.327 nm. Such a lattice was consistent with that reported in the literature.[29] The AFM image is illustrated in Figure 1C, and the BP-CdTe QDs presented an obvious lamellar structure with quantum dots attached, the height of BP-CdTe QDs was about 29.2 nm. The above results indicated that BP-CdTe QDs were successfully synthesized.

The chemical composition of BP-CdTe QDs was investigated by X-ray photoelectron spectroscopy. As depicted in Figure 1D, P 2p, C 1s, and O 1s exhibited their characteristic peaks at 132.92, 288.48, and 531.48 eV, respectively. Meanwhile, as seen from Figure 1E,F, the Cd 3d and Te 3d exhibited their characteristic peaks at 404.77 and 571.96 eV, respectively. The results of XPS also proved the preparation of BP-CdTe QDs.

ECL Mechanism of the Biosensor. To verify the improvement effect of BP nanosheet on the luminescence performance of CdTe QDs, the ECL signals of differently modified GCE were detected in 0.10 M PBS solution (pH 7.4) containing 10 mM TPrA with a potential scanning range of −1.5 to +1.2 V and the results are depicted in Figure 2A. For BP nanosheet modified GCE (curve *a*), no cathodic ECL emission was observed, but a weak anodic emission with 540 au was detected at +1.2 V, which was the ECL emission of BP nanosheet.[30] Although the CdTe QDs/GCE (curve *b*) had both an anodic ECL emission at +1.2 V and a cathodic emission at −1.5 V, their intensities were relatively weak, which were 2350 and 266 au, respectively. However, for the BP-CdTe QDs/GCE (curve *c*), the anodic and cathodic ECL emission intensities increased to 13 253 and 2783 au, which exhibited about 5.6-fold and 10.5-fold increase compared with that of CdTe QDs, respectively, indicating the improvement effect of BP nanosheet on the luminescence performance of CdTe QDs. The reason for the improvement effect of the BP nanosheet was as follows. On the one hand, the BP nanosheet has a large specific surface area, which could not only achieve high loading of CdTe QDs but also significantly increase the electroactive area. On the other hand, BP exhibited a high charge carrier mobility, which could increase the conductivity of the electrode interface and facilitate electron transfer. As a result, the ECL intensity of CdTe QDs was significantly improved because of the presence of the BP nanosheet.

The effect of H_2O_2 on both anodic and cathodic ECL emissions of BP-CdTe QDs was investigated (Figure 2B). The curve c in Figure 2B,A is the same, which was obtained in the presence TPrA alone. The curve *d* was detected at BP-CdTe QDs/GCE without TPrA and H_2O_2. In this case, only a weak cathodic emission was detected at −1.5 V, which was the ECL emission from CdTe QDs with dissolved O_2 as a co-reactant, and its intensity was the same as that of the cathodic signal in the curve *c*. The comparison of curves c and d indicated that TPrA was only an anodic co-reactant and has no effect on the cathodic emission of CdTe QDs. The curve e was detected at BP-CdTe QDs/GCE with TPrA and H_2O_2. In this case, the ECL signal from the cathode was significantly increased and the signal from the anode was effectively quenched, indicating that H_2O_2 was a superior dual-role moderator and could facilitate the different change of the two emissions.

The three-dimensional (3D) ECL spectra were further investigated. In the case of 10 mM TPrA as an anodic co-reactant, 3D ECL spectra of BP nanosheet, CdTe QDs, and BP-CdTe QDs modified GCE were detected. For BP/GCE (Figure 2C), only a weak anodic ECL emission was detected at +1.2 V and the maximum wavelength was located at 645 nm. As seen from Figure 2D, the CdTe QDs/GCE displayed the cathodic and anodic ECL emissions at −1.5 and +1.2 V, respectively, and both signals were weak, and the maximum wavelength of the two emissions was 704 nm. Figure 2E records the ECL spectrum of BP-CdTe QDs/GCE. The maximum wavelength of both the cathodic and anodic emissions was located at 709 nm, and their intensities increased significantly as compared to that of CdTe QDs. In addition, the 3D ECL spectrum BP-CdTe QDs/GCE was also detected in the presence of TPrA and H_2O_2 (Figure 2F). As expected, the anodic ECL emission of BP-CdTe QDs at +1.2 was effectively quenched (insets: enlarged anodic 3D ECL spectra) and the cathodic ECL emission at −1.5 V increased significantly. The above experimental facts indicated that both the cathodic and anodic ECL emissions in the case of BP-CdTe QDs were derived from CdTe QDs, and BP nanosheet could significantly enhance two emissions of CdTe QDs and H_2O_2 as a dual-role moderator could facilitate the different change in the two signals.

We also investigated whether there was resonance energy transfer (RET) between CdTe QDs and BP nanosheet. As seen from Figure S2, there was no obvious spectral overlap between the UV−vis absorption spectrum of CdTe QDs and the ECL spectrum of BP nanosheet, demonstrating that there was no RET between BP nanosheet and CdTe QDs.

The electron paramagnetic resonance (EPR) spectra with 2,2,6,6-tetramethyl-1-piperidinyloxy (TEMPO) as a trap were recorded to confirm that the hydroxyl radical (−OH) generated by H_2O_2 decomposition under light irradiation promoted the generation of photogenerated hole at BP-CdTe QDs, indicating that H_2O_2 could promote the cathodic ECL emission of BP-CdTe QDs. The corresponding figures (Figure

https://doi.org/10.1021/acs.analchem.1c02408
Anal. Chem. 2021, 93, 12400−12408

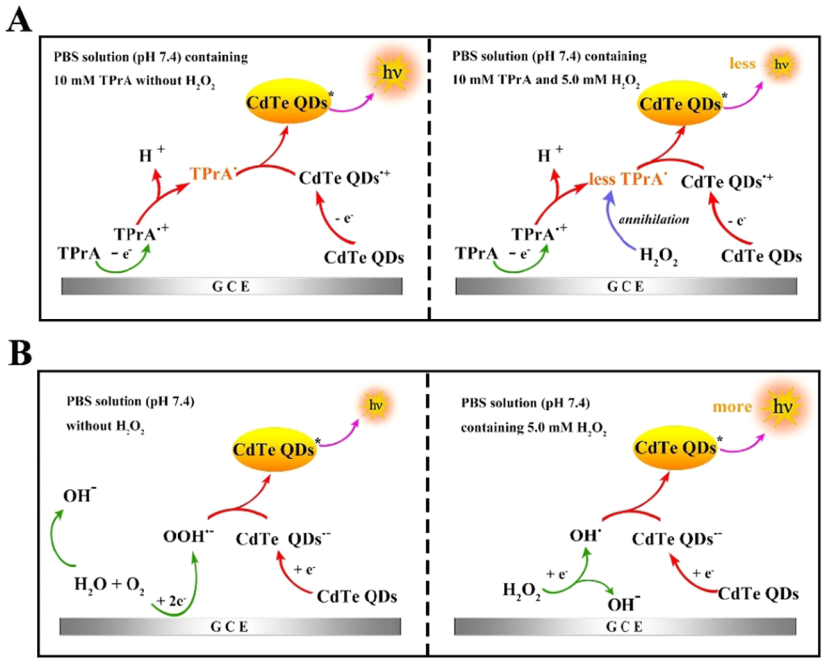

Figure 3. Mechanisms of H_2O_2 on (A) anodic and (B) cathodic ECL emissions of BP-CdTe QDs.

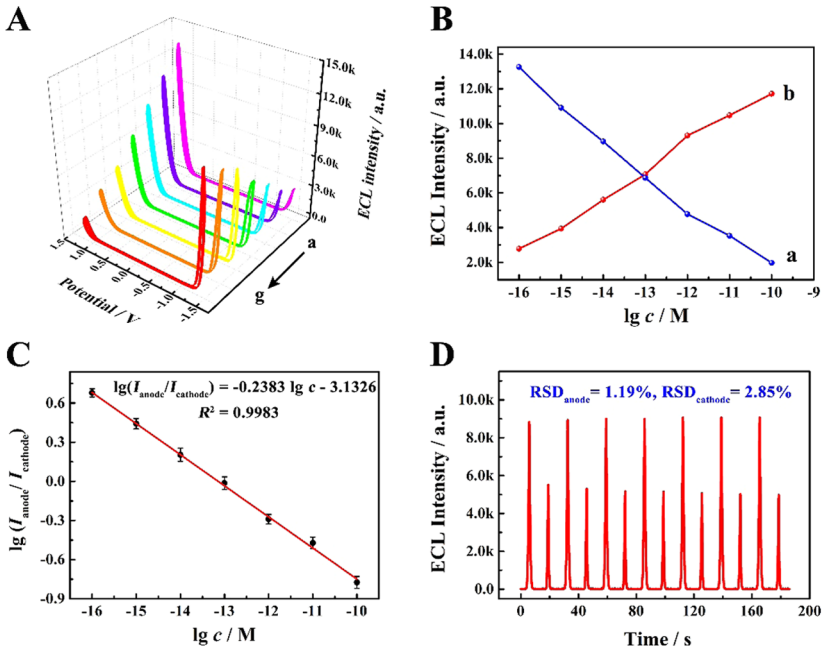

Figure 4. (A) ECL responses of the biosensor to miRNA-126, from (a) to (g): 100 aM, 1.0 fM, 10 fM, 100 fM, 1.0 pM, 10 pM, and 100 pM. (B) Change in I_{anode} (curve *a*) and $I_{cathode}$ (curve *b*) with the logarithm of miRNA-126 concentration. (C) The corresponding calibration plots between the logarithmic value of the ratio ($I_{anode}/I_{cathode}$) and the logarithm of miRNA-126 concentrations. (D) ECL stability of the biosensor with 1.0 fM miRNA-126. Detection solution: 0.10 M PBS solution (pH 7.4) containing 2.0 mM glucose and 10 mM TPrA. The voltage for the photomultiplier: 800 V. Scanning potential range: −1.5 to +1.2 V.

S3) and descriptions are displayed in the Supporting Information.

The mechanisms of H_2O_2 on anodic and cathodic ECL emissions of CdTe-TPrA are proposed as in Figure 3AB, respectively. In the absence of H_2O_2 (the left of Figure 3A), TPrA and CdTe QDs were electro-oxidized to produce $TPrA^{\bullet+}$ and CdTe $QDs^{\bullet+}$, respectively. The $TPrA^{\bullet+}$ was further transformed to $TPrA^{\bullet}$ through the deprotonation step. Then, $TPrA^{\bullet}$ reacted with CdTe $QDs^{\bullet+}$ to form CdTe QDs*, resulting in the anodic ECL emission. When H_2O_2 was present (the right of Figure 3B), the anodic ECL emission of BP-CdTe QDs was quenched due to the annihilation of $TPrA^{\bullet}$ radical by H_2O_2.[19] For the cathode process, in the absence of H_2O_2 (the left of Figure 3B), the dissolved O_2 as the co-reactant and H_2O were electroreduced to generate $OOH^{\bullet-}$, which would react with CdTe $QDs^{\bullet-}$ obtained from the electroreduction of CdTe QDs to produce CdTe QDs*, leading to a weak cathodic ECL emission.[31] In the presence of H_2O_2 (the right of Figure 3B),

https://doi.org/10.1021/acs.analchem.1c02408
Anal. Chem. 2021, 93, 12400−12408

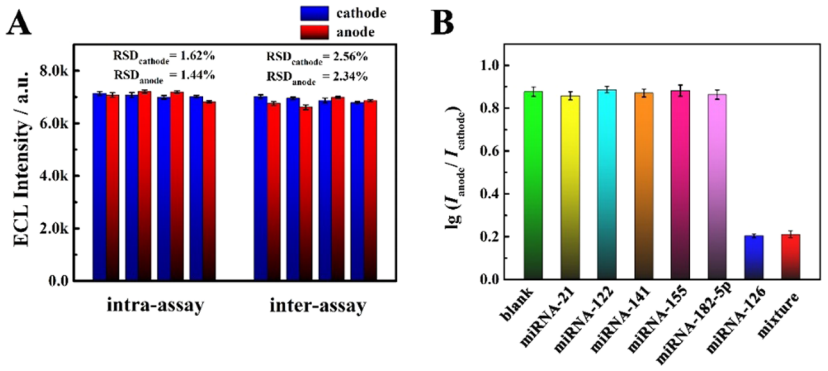

Figure 5. (A) Intra-assay and interassay reproducibilities of the biosensor incubated with 100 fM miRNA-126. (B) ECL responses of the biosensor to blank sample, miRNA-21 (100 fM), miRNA-122 (100 fM), miRNA-141 (100 fM), miRNA-155 (100 fM), miRNA-182-5p (100 fM), miRNA-126 (10 fM), and the mixed solution of above species.

the co-reactant H_2O_2 was electroreduced to produce $OH^•$, which reacted with CdTe $QDs^{•-}$ to produce the excited-state CdTe QDs*, resulting in a strong cathodic ECL emission.[18]

Native Polyacrylamide-Gel Electrophoresis (PAGE). The PAGE was performed, and Figure S4 depicts the corresponding results. The distinct bands were observed in lanes 1, 2, 3, 6, and 7, which corresponded to the target miRNA-126, H1, H2, circular template, and S1, respectively. Lane 4 was the band of the mixture of H1 and H2, illustrating that the hybridization of H1 and H2 was forbidden in the absence of target miRNA-126. For the mixture of H1, H2, and miRNA-126 (lane 5), an obvious band with slower migration was observed, which corresponded to the hybrids of H1 and H2, manifesting the CHA reaction among H1 and H2 in the presence of miRNA-126. The clear band on the top of lane 8 stood for the RCA products produced by the mixture of miRNA-126, H1, H2, and circular template. When S1 was further introduced into RCA products (line 9), the band on the top of line 9 was similar to that of lane 8 because the introduction of S1 did not cause significant changes in the relative molecular weight. Lane 10 was the band of the mixture of H1, H2, circular template, and S1, no band was observed on its top since the target miRNA-126 was absent and the RCA reaction was not initiated. The PAGE results demonstrated that the target recycling triggering RCA cascade nucleic acid amplification strategy was successfully established.

Optimization of Experimental Conditions. The RCA reaction time, glucose concentration, and scan rate were optimized and the corresponding figures (Figures S5 and S6) and descriptions are displayed in the Supporting Information. The optimal RCA reaction time, glucose concentration, and scan rate were 120 min, 2.0 mM, and 300 mV/s, respectively.

Detection of miRNA-126. The constructed biosensor was used for the quantitative measurement of miRNA-126 under optimal experimental conditions, and Figure 4A,B depicts the corresponding results. As the concentration of miRNA-126 went from 100 aM to 100 pM, the cathodic ECL signal increased while the anodic ECL emission decreased gradually. The corresponding linearity curve between the logarithmic value of the ratio ($I_{anode}/I_{cathode}$) and the logarithm of miRNA-126 concentrations is depicted in Figure 4C. The regression equation was $\lg(I_{anode}/I_{cathode}) = -0.2383 \lg c - 3.1326$ and the detection limit of 29 aM was obtained at S/N = 3. The performance comparison of our constructed biosensor and other reported methods for detecting microRNAs is illustrated in Table S2 in the Supporting Information, showing a lower detection limit of our biosensor.

Stability, Reproducibility, and Selectivity of Biosensor. First, the constructed biosensor was subjected to continuous cyclic scanning to evaluate its stability. As illustrated in Figure 4D, after seven cycles of cyclic scanning at 300 mV/s, the ECL responses to 10 fM miRNA-126 scarcely changed, and the anodic and cathodic ECL signals showed the relative standard deviations (RSDs) of 1.19 and 2.85%, respectively, indicating acceptable stability of the biosensor.

The reproducibility of the ECL biosensor was evaluated, and Figure 5A displays the results. Four biosensors prepared in the same batch were used to perform the intra-assay, and their cathodic and anodic ECL signals did not show significant changes. The calculated RSDs were 1.62 and 1.44%, respectively. Four biosensors prepared in the different batches were used to perform the interassay, and the RSDs of 2.56 and 2.34% were obtained for the cathodic and anodic ECL emissions, respectively. Those results showed that the developed biosensor had good reproducibility.

The influences of other miRNAs (miRNA-21, miRNA-122, miRNA-141, miRNA-155, and miRNA-182-5p) were further analyzed to evaluate the selectivity of the biosensor. As depicted in Figure 5B, the logarithmic value of ratio ($I_{anode}/I_{cathode}$) under blank sample, miRNA-21 (100 fM), miRNA-122 (100 fM), miRNA-141 (100 fM), miRNA-155 (100 fM), and miRNA-182-5p (100 fM) did not cause a significant interference on the ECL response. However, the target miRNA-126 (10 fM) and the mixture solution led to a significant decrease in the ratio ($I_{anode}/I_{cathode}$), indicating that the biosensor displayed a prominent specificity for miRNA-126.

Analysis of Real Serum Samples. The standard addition method was employed to assess the feasibility of the developed biosensor for clinical application. Briefly, miRNA-126 was added to the purified human serum, which was diluted to 50-fold with PBS solution (pH 7.4) to achieve a final concentration of 10.0 fM, 100 fM, 1.00 pM, and 10.0 pM. As listed in Table 1, the recoveries in four samples were 104, 98.8, 103, and 102%, respectively. Those results indicated that the designed biosensor possessed an excellent potential for clinical diagnosis.

CONCLUSIONS

In this work, BP nanosheet was innovatively developed to modulate CdTe QDs to simultaneously emit the cathodic and

https://doi.org/10.1021/acs.analchem.1c02408
Anal. Chem. 2021, 93, 12400−12408

Table 1. Analysis of Real Serum Samples

sample	added	found	RSD (%)	recovery (%)
1	10.0 fM	10.4 fM	2.7	104
2	100 fM	98.8 fM	4.4	98.8
3	1.00 pM	1.03 pM	1.5	103
4	10.0 pM	10.2 pM	3.2	102

anodic ECL signals, and H_2O_2 produced in situ by enzyme-catalyzed reaction and TPrA were chosen as the co-reactants of the two emissions, respectively. As a superior dual-role moderator, H_2O_2 facilitated the different variations in the two emissions. Our constructed biosensor exhibited excellent analytical performance for miRNA-126 detection. Because of the unique properties of the dual-ECL-emitting BP-CdTe QDs and dual co-reactant TPrA-H_2O_2, their combination provides a superior single-emitter-based ratio ECL sensing platform involving enzyme catalytic reaction and shows great application prospects in the analysis of diverse DNA, RNA, proteins, etc.

■ ASSOCIATED CONTENT

Supporting Information

The Supporting Information is available free of charge at https://pubs.acs.org/doi/10.1021/acs.analchem.1c02408.

Reagents and materials (Table S1); apparatus; CV and EIS characterization of the biosensor (Figure S1); UV−vis absorption spectra of CdTe QDs and ECL spectrum of BP nanosheets (Figure S2); EPR spectra of radical adducts in BP-CdTe QDs dispersion (Figure S3); native polyacrylamide-gel electrophoresis (Figure S4); optimization of experimental conditions (Figures S5 and S6); and comparison of different methods for microRNA detection (Table S2) (PDF)

■ AUTHOR INFORMATION

Corresponding Author

Shihong Chen − *Key Laboratory of Luminescence Analysis and Molecular Sensing (Southwest University), Ministry of Education, College of Chemistry and Chemical Engineering, Southwest University, Chongqing 400715, P. R. China;* orcid.org/0000-0001-7101-1223; Phone: +86-23-68253172; Email: cshong@swu.edu.cn

Authors

Jinwen Zhao − *Key Laboratory of Luminescence Analysis and Molecular Sensing (Southwest University), Ministry of Education, College of Chemistry and Chemical Engineering, Southwest University, Chongqing 400715, P. R. China*

Ying He − *Key Laboratory of Luminescence Analysis and Molecular Sensing (Southwest University), Ministry of Education, College of Chemistry and Chemical Engineering, Southwest University, Chongqing 400715, P. R. China*

Kejun Tan − *Key Laboratory of Luminescence Analysis and Molecular Sensing (Southwest University), Ministry of Education, College of Chemistry and Chemical Engineering, Southwest University, Chongqing 400715, P. R. China;* orcid.org/0000-0002-7704-4234

Jun Yang − *Key Laboratory of Luminescence Analysis and Molecular Sensing (Southwest University), Ministry of Education, College of Chemistry and Chemical Engineering, Southwest University, Chongqing 400715, P. R. China*

Ruo Yuan − *Key Laboratory of Luminescence Analysis and Molecular Sensing (Southwest University), Ministry of Education, College of Chemistry and Chemical Engineering, Southwest University, Chongqing 400715, P. R. China;* orcid.org/0000-0003-3664-6236

Complete contact information is available at: https://pubs.acs.org/10.1021/acs.analchem.1c02408

Notes

The authors declare no competing financial interest.

■ ACKNOWLEDGMENTS

This work was supported by the National Natural Science Foundation of China (21775122, 21775124, and 21705115) and the Natural Science Foundation of Chongqing City (cstc2018jcyjAX0693), China.

■ REFERENCES

(1) Liu, S. S.; Yuan, H. X.; Bai, H. T.; Zhang, P. B.; Lv, F. T.; Liu, L. B.; Dai, Z. H.; Bao, J. C.; Wang, S. *J. Am. Chem. Soc.* **2018**, *140*, 2284−2291.

(2) Yin, X.; Yang, P.; Zhang, H.; Zhu, Q.; Yuan, R.; Li, Y.; Liang, W. *Anal. Chem.* **2020**, *92*, 15120−15128.

(3) Zhang, G.; Chai, H.; Tian, M.; Zhu, S.; Qu, L.; Zhang, X. *Anal. Chem.* **2020**, *92*, 7354−7362.

(4) Zhou, H.; Ding, K.; Yu, Q.; Wang, H.; Liu, J.; Wang, Z. *Biosens. Bioelectron.* **2021**, *189*, No. 113367.

(5) Du, F.; Chen, Y.; Meng, C.; Lou, B.; Zhang, W.; Xu, G. *Curr. Opin. Electrochem.* **2021**, *28*, No. 100725.

(6) Han, Z.; Shu, J.; Liang, X.; Cui, H. *Anal. Chem.* **2019**, *91*, 12260−12267.

(7) Feng, Q.; Shen, Y.; Li, M.; Zhang, Z.; Zhao, W.; Xu, J.; Chen, H. *Anal. Chem.* **2016**, *88*, 937−944.

(8) Chen, H.; Zhang, H.; Yuan, R.; Chen, S. *Anal. Chem.* **2017**, *89*, 2823−2829.

(9) Du, D.; Shu, J.; Guo, M.; Haghighatbin, M. A.; Yang, D.; Bian, Z.; Cui, H. *Anal. Chem.* **2020**, *92*, 14113−14121.

(10) Chen, H.; Li, W.; Wang, Q.; Jin, X.; Nie, Z.; Yao, S. *Electrochim. Acta.* **2016**, *214*, 94−102.

(11) Chen, H.; Liu, X.; Yin, C.; Li, W.; Qin, X.; Chen, C. *Analyst* **2019**, *144*, 5215−5222.

(12) Cao, S.; Luo, Q.; Li, Y.; Liang, R.; Qiu, J. *Chem. Commun.* **2020**, *56*, 5625−5628.

(13) Wang, H.; Pu, G.; Devaramani, S.; Wang, Y.; Yang, Z.; Li, L.; Ma, X.; Lu, X. *Anal. Chem.* **2018**, *90*, 4871−4877.

(14) Huo, X.; Lu, H.; Xu, J.; Zhou, H.; Chen, H. *J. Mater. Chem. B* **2019**, *7*, 6469−6475.

(15) Zhang, C.; Liu, D.; Zhang, H.; Tan, X.; Chen, S. *Microchim. Acta* **2019**, *186*, No. 771.

(16) Fu, X.; Tan, X.; Yuan, R.; Chen, S. *Biosens. Bioelectron.* **2017**, *90*, 61−68.

(17) Hao, Q.; Wang, L.; Niu, S.; Ding, C.; Luo, X. *Anal. Chim. Acta* **2020**, *1136*, 134−140.

(18) Chen, H.; Liu, X.; Li, W.; Peng, Y.; Nie, Z. *Biosens. Bioelectron.* **2019**, *126*, 535−542.

(19) Feng, Q.; Guo, Y.; Xu, J.; Chen, H. *Biosens. Bioelectron.* **2018**, *100*, 571−576.

(20) Yu, Y.; Zhang, H.; Chai, Y.; Yuan, R.; Zhuo, Y. *Biosens. Bioelectron.* **2016**, *85*, 8−15.

(21) Ding, C.; Li, Y.; Wang, L.; Luo, X. *Anal. Chem.* **2019**, *91*, 983−989.

(22) Jiang, H.; Wang, X. *Anal. Chem.* **2014**, *86*, 6872−6878.

(23) Fu, L.; Zhang, B.; Fu, K.; Gao, X.; Zou, G. *Anal. Chem.* **2020**, *92*, 6144−6149.

(24) Li, M.; Feng, Q.; Zhou, Z.; Zhao, W.; Xu, J.; Chen, H. *Anal. Chem.* **2018**, *90*, 1340−1347.

(25) Xu, Y.; Wang, Z.; Guo, Z.; Huang, H.; Xiao, Q.; Zhang, H.; Yu, X. *Adv. Opt. Mater.* **2016**, *4*, 1223−1229.
(26) Jiang, Q.; Xu, L.; Chen, N.; Zhang, H.; Dai, L.; Wang, S. *Angew. Chem., Int. Ed.* **2016**, *55*, 13849−13853.
(27) Yang, Q.; Li, R.; Lyu, Q.; Hou, L.; Liu, Z.; Sun, Q.; Liu, M.; Shi, H.; Xu, B.; Yin, M.; et al. *Nat. Commun.* **2019**, *10*, No. 3389.
(28) Wang, S.; Aurora, A. B.; Johnson, B. A.; Qi, X.; McAnally, J.; Hill, J. A.; Richardson, J. A.; Bassel-Duby, R.; Olson, E. N. *Dev. Cell* **2008**, *15*, 261−271.
(29) Sun, M.; Liu, J.; Chai, Y.; Zhang, J.; Tang, Y.; Yuan, R. *Anal. Chem.* **2019**, *91*, 7765−7773.
(30) Gao, C.; Yu, H.; Wang, Y.; Liu, D.; Wen, T.; Zhang, L.; Ge, S.; Yu, J. *Anal. Chem.* **2020**, *92*, 6822−6826.
(31) Yang, X.; Yu, Y.; Peng, L.; Lei, Y.; Chai, Y.; Yuan, R.; Zhuo, Y. *Anal. Chem.* **2018**, *90*, 3995−4002.

https://doi.org/10.1021/acs.analchem.1c02408
Anal. Chem. 2021, 93, 12400−12408